THE JOURNAL OF
PHYSICAL CHEMISTRY C

Article

Bound Exciton and Optical Properties of SnO One-Dimensional Nanostructures

Weichang Zhou, Ruibin Liu, Qiang Wan, Qinglin Zhang, A. L. Pan, Lin Guo, and Bingsuo Zou

J. Phys. Chem. C, **2009**, 113 (5), 1719-1726• DOI: 10.1021/jp808422a • Publication Date (Web): 08 January 2009

The Journal of Physical Chemistry C is published by the American Chemical Society. 1155 Sixteenth Street N.W., Washington, DC 20036

J. Phys. Chem. C **2009,** *113,* 1719–1726

Bound Exciton and Optical Properties of SnO_2 One-Dimensional Nanostructures

Weichang Zhou,[†,§] Ruibin Liu,[†,§,#] Qiang Wan,*[,†] Qinglin Zhang,[†] A. L. Pan,[†] Lin Guo,[‡] and Bingsuo Zou*[,†]

State Key Laboratory for CBSC and Key Laboratory for Micro-Nano Opto-Electronic Devices of MOE, Hunan University, Changsha 410082, China, and Department of Materials Science and Engineering, Beijing University of Aeronautis and Astronatics, Beijing 100083, China

Received: September 22, 2008; Revised Manuscript Received: November 29, 2008

One-dimensional nanostructures of direct-forbidden semiconductor SnO_2 crystallite have been prepared in large scale via thermal evaporation of tin monoxide at 1100 °C. The anomalous optical emission even lasing phenomena are observed below the band edge under pulsed laser excitation, which usually does not occur for a direct-forbidden band semiconductor. Scanning electron microscopy, X-ray powder diffraction, transmission electron microscopy, UV−vis reflectance spectroscopy, and Raman scattering spectra were used to characterize the as-synthesized products. The processes of multiphonon coupling with exciton dominate in the exciton transition and lasing. The enhancement of exciton−phonon coupling and bound exciton transition could be mapped in the phonon scattering process. The origin of photoluminescence and lasing of SnO_2 nanobelts and nanowires was illustrated.

1. Introduction

One-dimensional (1D) and quasi-one-dimensional (quasi-1D) nanostructures are attracting a great deal of attention due to their unique properties and novel applications.[1] Semiconductor oxides are the basis of functional materials that have excellent properties and important technological applications. As an n-type semiconductor oxide with a wide band gap ($E_g = 3.6$ eV at 300 K), SnO_2 is well-known for its potential applications in dye-based solar cells,[2] photoconductors,[3] field-effect transistor,[4] gas sensors, and optical sensors.[5−8] A variety of 1D and quasi-1D nanostructures of SnO_2, such as nanobelts, nanowires, nanotubes, and nanorods,[4−10] have been fabricated successfully. Nanobelts, a new family in the realm of 1D nanomaterials, are regarded as an ideal system among these nanostructures to understand dimension-confined phenomena fully and may act as valuable units to construct nanodevices owing to their excellent properties.[10] Optical measurements such as photoluminescence (PL) and cathodoluminescence (CL) are very useful for the determination of the structures, defects, and impurities in nanostructures. There have been several reports on the luminescence of 1D SnO_2 nanostructures at room temperature,[11−16] showing emission in the range of 400−600 nm. Generally, these characteristics of luminescence are believed to stem from defects such as tin interstitials, dangling bonds, or oxygen vacancies. However, direct proof of such defects incorporated in the luminescence center has not yet been given. Law et al. reported the light waveguide properties in the visible region.[17] The investigation of the Raman scattering spectrum of SnO_2 particles shows that the appearance of infrared modes in the Raman scattering spectrum was due to phonon confinement effect and disorder because of the small size of crystals.[18] Wang et. al[19] provided new insights into the local structure−property relationship of SnO_2 nanoribbons by the combination of confocal Raman microspectroscopy with scanning electron microscopy (SEM). Their results can clearly discriminate the luminescent nanostructures on the nanoribbons surfaces, which can be attributed to defect state and exciton−phonon coupling.

In the present study, the optical properties of SnO_2 nanobelts are explored. The PL spectra of such nanobelts exhibit a strong emission band center at 555 nm with 325 nm CW laser excitation and two bands at 585 and 387 nm with pulsed laser excitation. Different from the nonresonance Raman scattering spectrum, the multiphonon process in SnO_2 nanobelts is shown up in the resonance Raman scattering spectrum. The mapping images of Raman scattering modes are in accord with the intensity of the corresponding modes in the nonresonance Raman scattering spectrum.

2. Experimental Section

Single crystal (1 cm × 1 cm), p-type Si(111) wafers were used as substrate in the study. The Si wafers were ultrasonically cleaned 10 min in acetone and ethanol, respectively. A 2 nm thick Au film was deposited at 4×10^{-6} Torr on these Si substrates at room temperature, which serves as the catalyst for growth nanostructures. Tin monoxide powder was placed in an alumina boat and covered with several pieces of Si wafers (the perpendicularity distance between the Si wafers and powder was 5 mm), then the boat was positioned in a quartz tube that was inserted into a horizontal alumina tube furnace. The furnace was heated to 1100 °C under Ar (99.99%) with a flow rate of 100 standard cubic centimeters per minute (sccm) at atmospheric pressure and held at that temperature for 2 h with unchanged the Ar flow rate. After being cooled down to room temperature, white wool-like products were formed on the Si substrates.

After the growth process, the resulting products were collected for phase identification by X-ray diffraction (XRD) using a D/max 5000 utilizing Cu Kα radiation. Morphological studies of the SnO_2 nanostructures were performed with a field emission scanning electron microscope (FE-SEM, JSM-6700F). The substrate-bound nanobelts were sonicated in ethanol and then

---

* To whom correspondence should be addressed. E-mail: bszou@hnu.cn (B.Z.), wanneo@gmail.com (Q.W.).

[†] Hunan University.

[‡] Beijing University of Aeronautis and Astronatics.

[§] These authors contributed equally to this work.

[#] Currently at Arizona State University.

10.1021/jp808422a CCC: $40.75

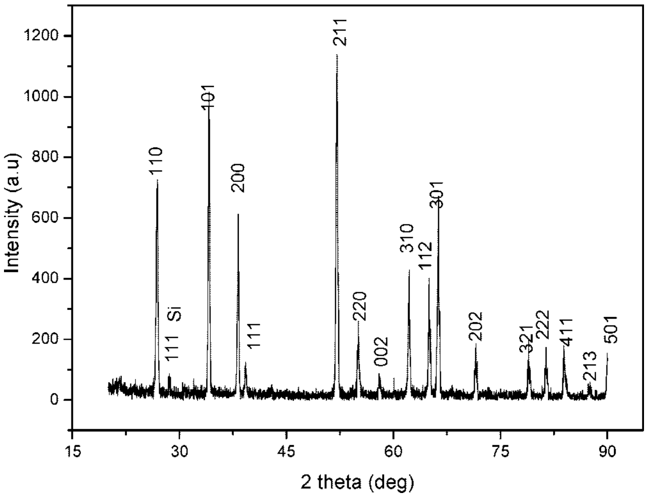

Figure 1. XRD pattern recorded from the as-synthesized products.

deposited on carbon-coated copper grids for transmission electron microscope (TEM, JEM-3010) characterization operating at 300 kV. The PL was excited by using a He−Cd laser with a wavelength of 325 nm, nanosecond laser pulse of 266 nm via a double SHG from a Nd:YAG laser, and femtosecond pulse of 266 nm from a Ti sapphire laser system as the excitation source at room temperature. The nonresonance Raman spectrum and mapping images were investigated by nearfield scanning optical microscopy (NSOM) excited by an Ar^+ laser (488 nm) at room temperature, whereas the resonance Raman spectrum was obtained with the excitation of a He−Cd laser.

3. Results and Discussion

The structure of the as-grown nanostructures was determined by XRD (as shown in Figure 1). All of the diffraction peaks, except one peak that comes from the Si substrate, can be ascribed to the tetragonal rutile SnO_2 structure with lattice constants of $a = 0.4742$ nm and $c = 0.3182$ nm (PDF 41-1445) and consist with the standard data file well.

Figure 2a is a low-magnification SEM image, which indicates that the as-synthesized products consist of a large quantity of 1D nanostructures. The representative high-magnification SEM image of several cross SnO_2 nanobelts, as shown in Figure 2b, can be produced at long time growth, which reveals that their geometrical shape is beltlike and uniform in size. The typical nanobelt is a few tens of nanometers in thickness, a few hundreds of nanometers in width, and several hundreds of micrometers in length. No catalyst is observed at the tip of the nanobelts due to that the Au particle are pulled off when growth is completed. For the short time growth, we can obtain SnO_2 nanowires. The in situ energy-dispersive X-ray spectrum (EDS) (see the inset of Figure 2b), which attach on SEM, shows that the sample contains only elemental O and Sn, except for the element Si which comes from the substrate, and the atomic ratio of O/Sn is about 2.6. Some excessive O element may come from air remaining in the vacuum chamber of the SEM or SiO_2 covering on the Si substrate.

The nanobelts were further characterized with TEM and high-resolution TEM (HRTEM). Figure 3a shows a typical TEM image of two intersecting SnO_2 nanowires with 150 nm width. Figure 3b is the HRTEM image of a SnO_2 nanobelt, which indicates their high crystallinity. The corresponding selected area electron diffraction (SAED) pattern (see the inset in Figure 3b) confirms the tetragonal rutile phase structure and single-crystalline nature. The lattice planes of (101) and (220) can be determined from the SAED pattern, and the growth directions of SnO_2 nanobelts are [101] and [110] of transverse direction and longitudinal direction, respectively. The angle of the crystal stripe between the transverse and longitudinal directions is 68°, which is close to the angle between the crystal lattice (101) and (110). The formation of SnO_2 nanobelts should be related to a vapor−liquid−solid (VLS) plus vapor−solid (VS) mechanism.[20,21] The growth follows the VLS process which is guided by the Au particle at the initial growth stage, which gives the nanowires. Just the VLS mechanism cannot completely account for the formation of nanobelts, since their transverse sizes become large during the growth. The VS process contributes to the formation of nanobelts. That is, SnO_2 nanowires form and grow in the longitudinal direction via the VLS process at the initial stage, then some vapor of Sn and O_2 could epitaxially deposit onto the side surfaces of the nanowires via the VS process due to the high temperature and second reactivity of the early formed nanowires and finally lead to the nanobelts. Due to the longer growth time, the nanobelts are in the size of 120−500 nm width and 25−80 nm thickness, whereas the nanowires are 40−130 nm in thickness. This two-process mechanism is ever reported on the growth of CdSSe,[22] CdSe[23] nanobelts, and many others.

Figure 3c is the HRTEM of SnO_2 nanowires in varied view directions, even the monocrystalline structure; we can find many nanosized substructures on the surface of the nanowire. Clearly these substructures are caused by the Sn drop in the fast growth of nanowires at the early stage. These structures indicate that the growth process at the early stage is not uniform with steady precursor supply, which induces a lot of defects formed on the surface of the nanowires. The nanobelts show better crystalline structure for their longer growth time. This structural difference may cause the varying optical responses.

The UV−vis reflectance spectra of SnO_2 nanowires has been obtained for nanowires and nanobelts (see Figure 4a); they did not show a clear difference in the whole profile. For the nanobelt the spectrum gives a slightly sharp band edge in the range of 3.5−3.0 eV (Figure 4b). We fitted the spectra with the Gaussian lines, which give good agreement with the early reports on the electronic structure and spectroscopic data of SnO_2 crystals.[24] The lowest direct transition $\Gamma_5^+ \rightarrow \Gamma_1^+$ is at 3.68 eV and a slightly higher band $\Gamma_1^- \rightarrow \Gamma_1^+$ is at 4.07 eV; these two strong bands can be found in Figure 4 to be the fitted lines 2 (4.22 eV) and 3 (3.73 eV). Line 1 is a higher band at the Γ point. Below the first direct band there is a clear exciton series at about 3.59 eV,[24] which agrees perfectly with line 4. Below the exciton transition, there may exist a weak band due to impurities or defects in the range of 3.3−3.0 eV, which is due to the bound exciton.[24] Our fitted line 5 for this bound exciton is centered at 3.223 eV. The intensity of line 5 is slightly weaker for nanobelts than that of nanowires, which may indicate a lower density of state (DOS) for bound excitons. Within the band gap the deeptrap centers are distributed in the energy range of 2.6−1.8 eV, which is fitted for line 6. For nanobelts, the locations of the line 1 and 2 bands move around due to their high continuum band characteristics. The first direct band $\Gamma_5^+ \rightarrow \Gamma_1^+$ transition is fitted at around 3.66 eV; its free exciton line cannot be fitted out for its forbidden nature. The bound exciton line moves slightly to 3.28 eV with much smaller intensity. The deeptrap band shows a weak broad band between 2.89 and 1.9 eV. These fitted lines coincided well with the reported electronic structure of crystalline SnO_2.

Optical measurements such as PL are very useful to determination the structures, defects, and impurities in nanostructures.

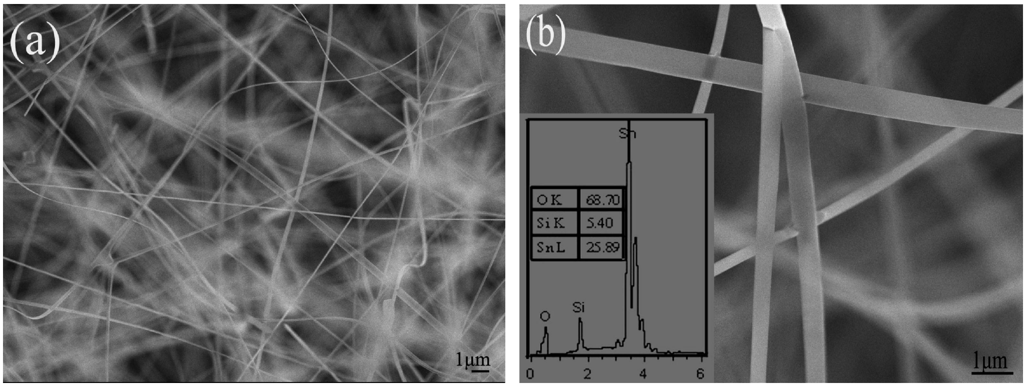

Figure 2. Typical SEM images of the as-synthesized products: (a) low-magnification image; (b) high-magnification image; the inset is the energy-dispersive X-ray spectrum (EDS) of the nanobelts.

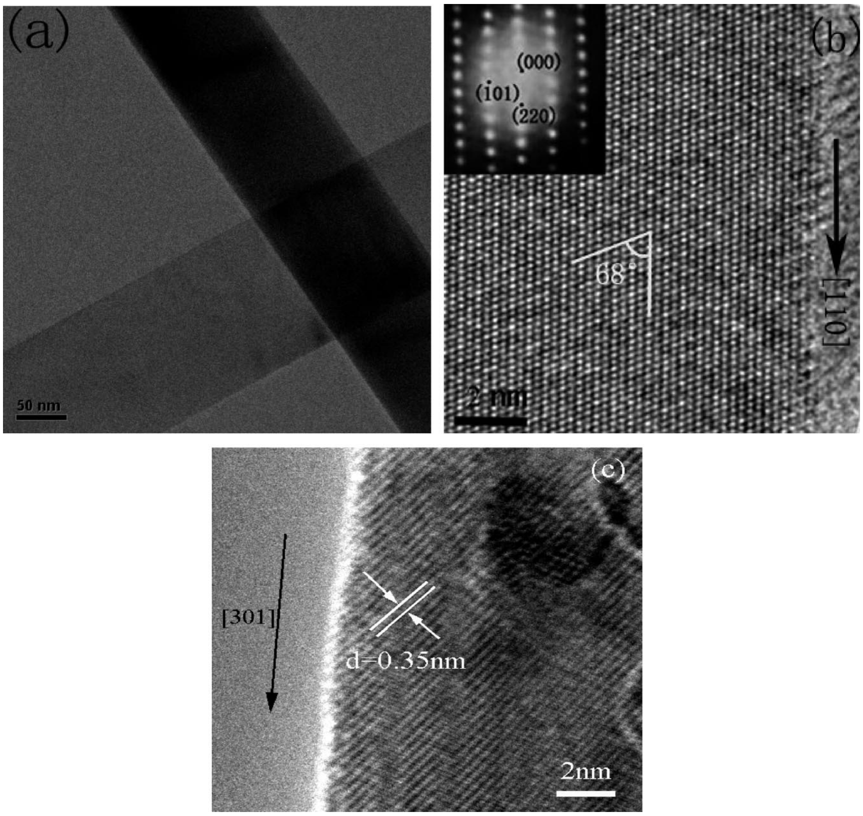

Figure 3. TEM images of SnO_2 nanobelts: (a) typical TEM image of two intersecting SnO_2 nanobelts; (b) HRTEM lattice image; the inset shows its corresponding SAED pattern. (c) HRTEM of nanowires at varied view directions.

Figure 5A shows the PL spectrum of the as-prepared SnO_2 nanobelts by 325 nm CW laser light excitation at room temperature. A yellow broad emission band located at 555 nm (2.24 eV) is observed, and it is apparent that the broad peak is the result of the convolution of more than one emission line. This band shifts from 555 nm for nanowires to 590 nm for nanobelts, which is related to deeptrap. The near band edge (NBE) emission (exciton, expected around 350 nm) is not detected in this measurement because of the dipole-forbidden nature of first transition for SnO_2.[24] First-principle calculation shows that the oxygen vacancy (O_V) and tin interstitial (Sn_I) have surprisingly low formation energies and strong mutual attractions;[25] therefore, O_V and Sn_I can form easily while it is not energetically costly in SnO_2 lattices. These defects of high concentration can exist and act as traps for long-range carriers and lead to the formation of a large amount of trapped states within the band gap, which results in the strong green emission signal. These states also are related to the proximity to metal conductivity with visible transparency. There are already some other reports about the PL emission bands of SnO_2 in the range of 400−600 nm, which are ascribed to the crystalline defects or surface states in nanostructures.[11,12,15] Figure 5B shows the PL spectrum of SnO_2 nanobelts/nanowires under illumination of a 266 nm nanosecond pulse; the emission spectrum gives two bands at 587 and 387.5 nm from bound exciton and deeptrap, respectively. Figure 5C shows the emission spectrum of nanobelts under 266 nm femtosecond pulse excitation of power fluence below 15 μJ; Figure 5d shows the emission spectra of nanowires at excitation above 15 μJ. The emission band goes to narrow when the excitation power is increased to 50 μJ, which goes broader when the excitation power rises to above 60 μJ. The power-dependent emission intensities of nanowires and nanobelts are shown in Figure 5e. The stimulated emission occurs at high power (Figure 5d) for both nanowires and belts; their emission spectral profiles change with similar way, like that has been reported in ref 26. It is interesting that

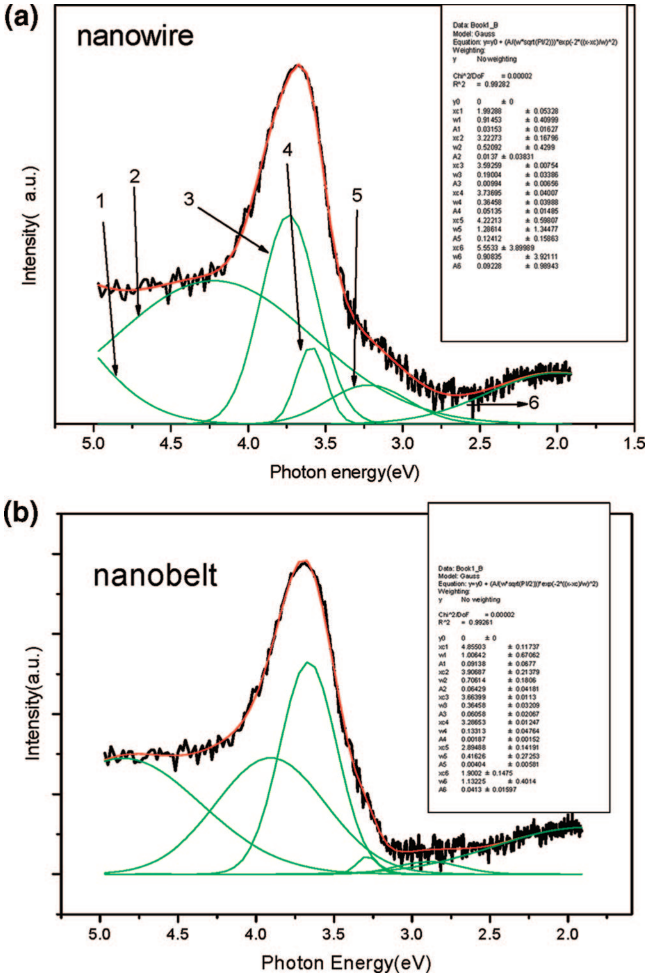

Figure 4. (a and b) Reflectance spectra of SnO_2 nanowires and nanobelts.

the UV emission always occurs at femtosecond pulsed laser excitation, which usually happens at the energy of bound exciton with finite lifetime for SnO_2 nanowires or nanobelts of low defect or doping concentration. For the highly doped nanowire, their emission is very low and shows no stimulated emission. That is because too much scattering blocked the light transport in the 1D nanostructure. For the nanowire and nanobelt have different sizes and microstructures, so their steady-state DOS of bound exciton is different, which leads to varied lasing threshold in Figure 5e. Small size leads to less threshold for lasing, which is supported by our data of nanowires and nanobelts, but we cannot determine its limitation of size effects. The effect of defect concentration to emission is definite; however, high density defects cannot produce stimulated emission at all but only broad emission due to the conductivity effect. If the excitation power reaches a higher value than the threshold, the stimulated emission intensity become saturated, their bandwidth would become broadened, especially for the nanowire, which is clearly due to the enhancement of lattice vibration contribution in the optical transition. This result is in agreement with the optical absorption in Figure 4, parts a and b.

A weak and narrow emission band of free exciton at 3.61 eV can only be found surprisingly at the femtosecond pulse excitation at low fluence, which disappeared when the stimulated emission came out. But this exciton emission line is not detected for nanobelts. Such phenomena should be that its appearance depends upon its lifetime. Its short lifetime due to forbidden transition cannot support its observance at nanosecond and CW excitation. Its disappearance at stimulated emission of bound exciton should be related to that the free exciton may transform swiftly into bound exciton via phonon assistance at defects, which will be discussed later. The intensity of yellow deeptrap emission increases slightly with femtosecond laser power while the UV emission increases dramatically to reach stimulated emission. The threshold power for stimulated emission for nanobelts is clearly larger than that for nanowires; sometimes we even cannot see stimulated emission for longer and broader nanobelts, which possibly is due to less defects of them. One can easily see this for their different DOS of bound excitons in nanobelts and nanowires (see Figure 4, parts a and b), for bound exciton is related to the free exciton coupling with defects.

Raman scattering spectra of SnO_2 nanobelts and nanowires are studied to understand the exciton−phonon coupling and bound exciton formation. Parts a and b of Figure 6 show the Raman scattering spectrum of as-synthesized SnO_2 nanobelts at room temperature. Rutile SnO_2 belongs to the point group D_{4h}^{14} and space group $P4_2/mnm$. The unit cell consists of two metal (Sn) atoms and four oxygen atoms, in which each metal atom is situated amidst six oxygen atoms which approximately form the corners of a regular octahedron while oxygen atoms are surrounded by three tin atoms which are close to the corners of an equilateral triangle (see Figure 6c). The normal lattice vibration modes at the Γ point of the Brillouin zone are given on the basis of group theory:[27] $\Gamma = 1A_{1g}(\Gamma_1^+) + 1A_{2g}(\Gamma_2^+) + 2A_{2u}(\Gamma_1^-) + 1B_{1g}(\Gamma_3^+) + 1B_{2g}(\Gamma_4^+) + 2B_{1u}(\Gamma_4^-) + 1E_g(\Gamma_5^-) + 4E_u(\Gamma_5^+)$. Among them, the active Raman modes are B_{1g}, E_g, A_{1g}, B_{2g}; therefore, four first-order Raman spectra are observed and the vibration intensity of the A_{1g} mode is the strongest, followed by the E_g; the modes of A_{2u} and E_u are IR-active, whereas A_{2g} and B_{1u} are inactive modes.

Figure 6a shows the nonresonant Raman scattering (RS) spectrum of a single SnO_2 nanobelt and Figure 7 shows the Raman mapping imaging of each corresponding Raman scattering vibration mode. From the nonresonance Raman spectrum (excitation by 488 nm of Ar^+ laser), we can only observe two vibration modes A_{1g} 633 cm^{-1} and B_{2g} 772 cm^{-1}, whereas the E_g mode is too weak to be observed. The two nondegenerate normal phonon modes, A_{1g} and B_{2g}, are related to the expansion and contraction vibration of Sn−O bonds (vibrate in the plane perpendicular to the *c*-axis), respectively (see Figure 6d); the E_g phonon mode is a nonpolar mode, and only two oxygen atoms vibrate out of phase along the *Z*-axis while the other two oxygen atoms fix (see Figure 6d). No new or extra peak occurs, which indicates that the phase in the nanobelt or nanowire is typical SnO_2 with no clear impurities.

In the resonant Raman scattering (RRS) spectrum (Figure 6b), there are three strong Raman scattering peaks, 475, 634, 773 cm^{-1}, corresponding to the E_g, A_{1g}, and B_{2g} modes, respectively, with some background. Some two-phonon (overtone) modes enhance when 325 nm light excites the 1s or np exciton states (3.59 eV or above) for SnO_2 nanobelts. They need phonons to assist its radiative transition. For the large energy span (0.39 eV) between free exciton and bound exciton, a single phonon cannot cover this span for their limited energies. In the radiative transition process of the SnO_2 1D nanostructure, the photoinduced excitons can propagate along the longitudinal axis with long length, which certainly produces enhanced coupling between exciton and phonon via Fröhlich long-range interaction. This coupling can induce a multiphonon transition via the local deformation. So the resonant enhanced modes of 972 ($E_g + E_g$), 1112 ($E_g + A_{1g}$), 1255 ($A_{1g} + A_{1g}$), 1382 ($A_{1g} + B_{2g}$), and 1509 ($B_{2g} + B_{2g}$) cm^{-1} are necessarily observed for their

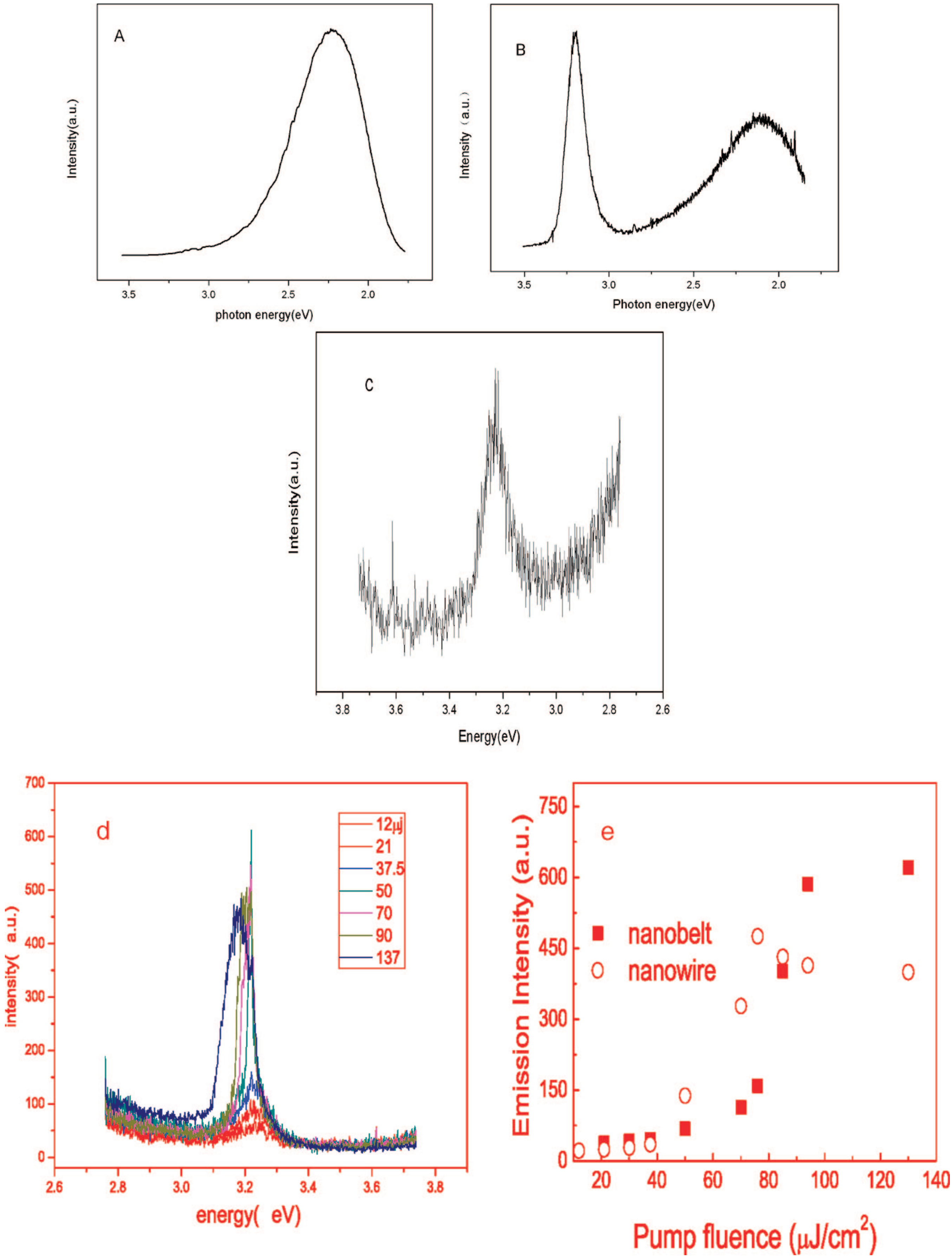

Figure 5. Normalized PL spectra of obtained SnO_2 nanowires and belts.

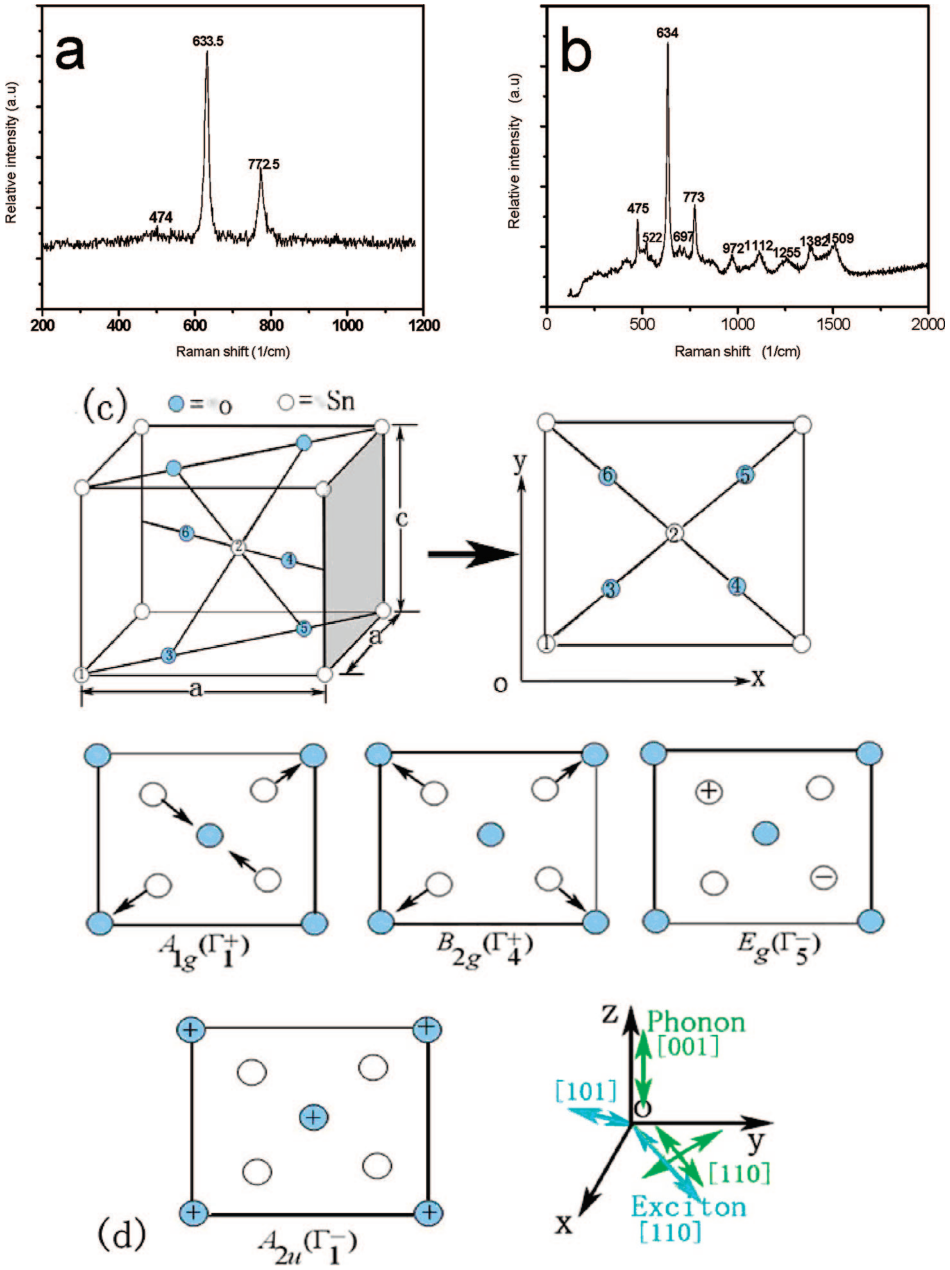

Figure 6. Raman spectrum of the as-synthesized SnO_2 nanobelts: (a) resonance Raman spectrum; (b) nonresonance Raman spectrum; (c) rutile structure of a SnO_2 crystal and projection image in the *xoy* plane; (d) symmetry of the optic modes of SnO_2 structure for zero wave vector and transport orientation of excitons and lattice vibration direction of phonons, respectively.

complicated orientations. These modes all have their projection components to the long axial direction of the nanowire and nanobelt, so they all can contribute to the coupling to excitons transported in the nanowire or nanobelt. Usually the multiphonon peaks are related to the bound excitons or trapped excitons due to an enhanced exciton−phonon coupling in the nanostructure or system with impurity.[28−30]

There have been reports that the intensity ratio between the second- and first-order Raman scattering is closely proportional to the electron−phonon coupling strength and symmetry selection,[28] and the 1D structure with large aspect ratio will enhance the nonlinear coupling between exciton and phonon;[29] therefore, this multiphonon phenomenon is related to the defects and impurities which bind free excitons to produce bound exciton under resonant excitation. The existence of crystalline defects or surface states in SnO_2 nanobelts and nanowires (see PL in Figure 5) would induce localized deformation potential for trapping and dissociation of free excitons. The dissociation of free exciton may produce itinerant carriers, which may cause the background in the RRS spectra and screen some of the multiphonons. That is why the multiphonon energies in Figure 6b are slightly less than the summation values of related two phonons. If the carrier is bound to local structures or impurities without motion, it is generally the energy very close to the summation of two phonons. Deeptrap also supports multiphonon scattering,[30] which is evidenced by the visible emission of SnO_2 nanobelts and nanowires under excitations.

On the basis of the above analysis we can deduce that the 385 nm emission originates from bound exciton, which is bound to some impurities or defect weakly and can move to an extent at room temperature. In the nanowires and nanobelts, the bound exciton motion may be also assisted by itinerant carriers. When bound excitons move in the 1D structure with a definite number after femtosecond excitation, the numerous bound excitons may

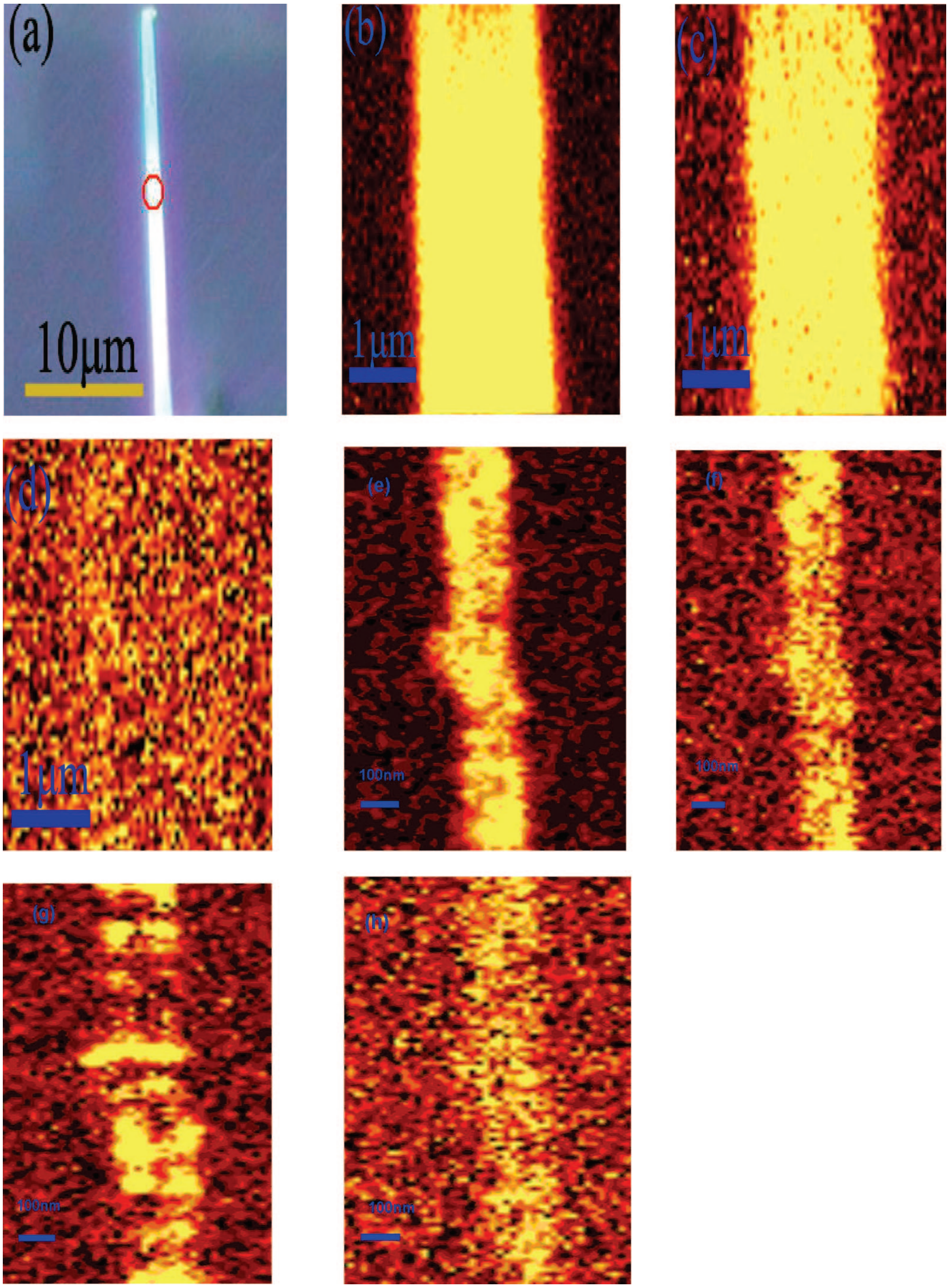

Figure 7. (a) Morphology image of a SnO_2 nanobelt which was selected for the nonresonance Raman spectrum. (b−d) The corresponding mapping images of the A_{1g}, B_{2g}, and E_g modes under nonresonant excitation, respectively. (e−h) The mapping image of E_g, and 1509 cm^{-1} ($B_{2g} + B_{2g}$), 972 cm^{-1} ($2E_g$), and 1255 cm^{-1} ($E_g + A_{1g}$) of a SnO_2 nanowire under resonant excitation, respectively.

overlap to lead to a giant oscillator strength and emit collectively because the 1D structure is a natural Fabry−Perot cavity. This coherent radiation behavior depends on the lifetime of these bound excitons. Nanobelts with less surface roughness or defects need higher femtosecond laser fluence than nanowires for their lower efficiency of photonic harmonic oscillation in the cavity. It is easy to reach lasing in a nanowire of longitudinal axial to one crystal axis. The orientation of exciton motion can be seen in the HRTEM image (Figure 3b) of nanobelts, in which the transverse and longitudinal axis directions of the nanobelt are [101] and [110], respectively. That is, the moving directions of excitons in SnO_2 nanobelts are along [101] and [110], respectively. The lattice vibration directions of the A_{1g} and B_{2g} modes are along ±[110], whereas the direction of E_g is along ±[001] (Figure 6d). These phonon vibrating directions are not perpendicular to the exciton motion directions (long axial of the wire) of bound exciton, so they all can polarize with that of bound excitons via the projectual components of phonons, i.e., many phonons with different orientations may all contribute to dephase the exciton coherence, lifting the lasing threshold. In the meanwhile the electron−hole plasma might be incurred at high power, evidenced by the saturation of emission and band broadening[26] in SnO_2 nanowires. In earlier reports, a large density of the 2LO phonon-coupled excitons in nanowires is responsible for the stimulated emission of single CdS nanoribbons,[31] Mn-doped ZnO nanowires,[32] and GaN nanowires[33] at room temperature, respectively. Such a two-phonon bound state in the as-synthesized SnO_2 nanobelts or nanowires may also assist to achieve stimulated emission. The 1D Fabry–Parot cavity and optical waveguide are crucial for the realization of stimulated emission from bound excitons along the axis of 1D nanostructures.[26,34,35]

The excess dopings or defects in SnO_2 nanowires and nanobelts cannot realize lasing phenomena, for the carriers but not bound exciton dominated their optical behaviors. This situation is beyond the range of our discussion here.

In addition to those Raman modes, there are two new modes observed at 522 and 697 cm^{-1} under resonant excitation, which are close to the IR-active mode of A_{2u}(TO) at 512 cm^{-1} and A_{2u}(LO) at 687 cm^{-1}, respectively, according to theoretical calculation.[36] The defects in SnO_2 nanobelts such as vacancies of oxygen, vacancy clusters, and local lattice disorder (see the PL spectra in Figure 5) at the interface and interior surface may lead to a significant enhanced carrier–phonon coupling with carrier propagation in 1D nanowires, which would result in relaxation of the selection rule, and therefore some IR modes can be observed in the RRS spectrum.

The Raman mapping images (Figure 7b–d) of a single SnO_2 nanobelt show the signal strength of the A_{1g} mode is the strongest following by the B_{2g} mode, whereas the signal strength of E_g can almost not be observed, which is according with the Raman scattering spectrum intensities. These mapping images suggest that there is not any contamination adsorption on the as-synthesized SnO_2 nanobelts. The Raman mapping images (Figure 7e–h) of a single nanowire (110 nm) is obtained under resonant excitation. The strongest and second strong peaks are still A_{1g} and B_{2g} modes, but the E_g mode is enhanced significantly, together with the multiphonon modes. Moreover the latter exhibited an intensity fluctuation along the longitudinal axis, which indicated a structural fluctuation. These mode enhancements reflected the exciton and phonon coupling mechanism in their respective orientations.

4. Conclusion

In summary, SnO_2 nanobelts and nanowires have been synthesized by thermal evaporation of SnO powder at atmospheric pressure. Their microstructures and compositions are characterized. The as-synthesized nanostructures show a broad strong emission band at 555 nm under CW laser excitation at room temperature due to the crystalline defect levels associated with oxygen vacancies or trapped states. The resonant Raman spectrum reveals that SnO_2 nanobelts or nanowires produce a multiphonon process when excited by 325 nm of a He–Cd laser, which indicated the varied orientational couplings between exciton and phonons, reflected the origin of bound exciton and deeptrap transitions. These 1D SnO_2 nanostructures may produce stimulated emission with some size effect through the cooperative emission of the bound excitons, which may find application in nanolasers. This work also helps to understand the exciton transition in indirect or direct-forbidden semiconductor 1D nanostructures.

Acknowledgment. We thank the NSFC of China (term nos. 90606001, 50602015, 50725208, and 90406024) and Hunan Provincial Natural Science Foundation (07jj4002) for financial support.

References and Notes

(1) *Nanowires and Nanobelts*; Wang, Z. L., Ed.; Kluwer Academic: New York, 2003; Vols. *I* (Metal and Semiconductor Nanowires) and *II* (Nanowires and Nanobelts of Functional Materials).

(2) Ferrere, S.; Zaban, A.; Gsegg, B. A. *J. Phys. Chem. B* **1997**, *101*, 4490.

(3) Mathur, S.; Barth, S.; Shen, H.; Pyun, J. C.; Werner, U. *Small* **2005**, *1*, 713.

(4) Zhang, Y.; Kolmakov, A.; Chretien, S.; Metiu, H.; Moskovits, M. *Nano Lett.* **2004**, *4*, 403.

(5) Kolmakov, A.; Klenov, D. O.; Stemmer, S.; Moskovits, M. *Nano Lett.* **2005**, *5*, 667.

(6) Wang, Z. L. *Adv. Mater.* **2003**, *15*, 432.

(7) Sirbuly, D. J.; Tao, A.; Yang, P. D. *Adv. Mater.* **2007**, *19*, 61.

(8) Dai, Z. R.; Gole, J. L.; Stout, J. D.; Wang, Z. L. *J. Phys. Chem. B* **2002**, *106*, 1274.

(9) Xu, C. K.; Zhao, X. L.; Liu, S.; Wang, G. H. *Solid State Commun.* **2003**, *125*, 301.

(10) Pan, Z. W.; Dai, Z. R.; Wang, Z. L. *Science* **2001**, *291*, 1947.

(11) Hu, J. Q.; Ma, X. L.; Shang, N. G.; Xie, Z. Y.; Wong, N. B.; Lee, C. S.; Lee, S. T. *J. Phys. Chem. B* **2002**, *106*, 3823.

(12) Luo, S. H.; Fan, J. Y.; Chu, P. K. *Nanotechnology* **2006**, *17*, 1695.

(13) Zhou, X. T.; Regier, T.; Sham, T. K. *Appl. Phys. Lett.* **2006**, *89*, 213109.

(14) Faglia, G.; Baratto, C.; Sberveglieri, G.; Zha, M.; Zappettini, A. *Appl. Phys. Lett.* **2005**, *86*, 011923.

(15) He, J. H.; Wu, T. H.; Wang, Z. L. *Small* **2006**, *1*, 116.

(16) Maestre, D.; Cremades, A.; Piqueras, J. *J. Appl. Phys.* **2005**, *97*, 044316.

(17) Law, M.; Sirbuly, D.; Johnson, J.; Goldberger, J.; Saykally, R.; Yang, P. *Science* **2004**, *305*, 1269.

(18) Diéguez, A.; Romano-Rodríguez, A.; Vilà, A.; Morante, J. R. *J. Appl. Phys.* **2001**, *90*, 1550.

(19) Wang, F. P.; Zhou, X. T.; Zhou, J. G.; Sham, T. K.; Ding, Z. F. *J. Phys. Chem. C* **2007**, *111*, 18839.

(20) Wagner, R. S.; Ellis, W. C. *Appl. Phys. Lett.* **1964**, *4*, 89.

(21) Brenner, S. S.; Sears, G. W. *Acta Mater.* **1956**, *4*, 268.

(22) Pan, A. L.; Yang, H.; Yu, R. C.; Zou, B. S. *Nanotechnology* **2006**, *17*, 1083.

(23) Venugopal, R.; Lin, P.; Liu, C.; Chen, Y. *J. Am. Chem. Soc.* **2005**, *127*, 11262.

(24) Agekyan, V. T. *Phys. Status Solidi A* **1977**, *43*, 11.

(25) Kılıç, Ç.; Zunger, A. *Phys. Rev. Lett.* **2002**, *88*, 095501.

(26) Liu, R. B.; Chen, Y. J.; Wang, F. F.; Cao, L.; Pan, A. L.; Yang, G. Z.; Wang, T. H.; Zou, B. S. *Physica E* **2007**, *39*, 223.

(27) (a) Katiyar, R. S. *J. Phys. C* **1970**, *3*, 1087. (b) Traylor, J. G.; Smith, H. G.; Nicklow, R. M.; Wilkinson, M. K. *Phys. Rev. B* **1971**, *3*, 3457.

(28) Wang, R. P.; Xu, G.; Jin, P. *Phys. Rev. B* **2004**, *69*, 113303.

(29) Mahan, G. D.; Gupta, R.; Xiong, Q.; Adu, C. K.; Eklund, P. C. *Phys. Rev. B* **2003**, *68*, 073402.

(30) (a) Riera, R.; Rosas, R.; Marín, J. L.; Bergues, J. M.; Campoy, G. *J. Phys.: Condens. Matter* **2003**, *15*, 3225. (b) Ursaki, V. V.; Tiginyanu, I. M.; Zalamai, V. V.; Rusu, E. V.; Emelchenko, G. A.; Masalov, V. M.; Samarov, E. N. *Phys. Rev. B* **2004**, *70*, 155204.

(31) Pan, A. L.; Liu, R. B.; Zou, B. S. *Appl. Phys. Lett.* **2006**, *88*, 173102.

(32) Liu, R. B.; Pan, A. L.; Fan, H. M.; Wang, F. F.; Shen, Z. X.; Yang, G. Z.; Xie, S. S.; Zou, B. S. *J. Phys.: Condens. Matter* **2007**, *19*, 136206.

(33) Dhara, S.; Chandra, S.; Mangamma, G.; Kalavathi, S.; Shankar, P.; Nair, K. G. M.; Tyagi, A. K.; Hsu, C. W.; Kuo, C. C.; Chen, L. C.; Chen, K. H.; Sriram, K. K. *Appl. Phys. Lett.* **2007**, *90*, 213104.

(34) Huang, M. H.; Mao, S.; Feick, H.; Yan, H.; Wu, Y.; Kind, H.; Weber, E.; Russo, R.; Yang, P. D. *Science* **2001**, *292*, 1897.

(35) (a) Pan, A. L.; Liu, R. B.; Zou, B. S. *J. Phys. Chem. B* **2005**, *109*, 24268. (b) Pan, A. L.; Liu, R. B.; Wang, F. F.; Xie, S. S.; Zou, B. S.; Zacharias, M.; Wang, Z. L. *J. Phys. Chem. B* **2006**, *110*, 22313. (c) Pan, A. L.; Liu, R. B.; Zhang, Q. L.; Wan, Q.; He, P. B.; Zacharias, M.; Zou, B. S. *J. Phys. Chem. C* **2007**, *111*, 14253.

(36) Katiyar, R. S.; Dawson, P.; Hargreave, M. M.; Wilkinson, G. R. *J. Phys: Condens. Matter* **1971**, *4*, 2421.

JP808422A